

A CONTRACTING, TURBULENT, STARLESS CORE IN THE SERPENS CLUSTER

Jonathan P. Williams¹ and Philip C. Myers

Harvard-Smithsonian Center for Astrophysics, 60 Garden Street, Cambridge, MA 02138;
 jpw@cfa.harvard.edu, pmyers@cfa.harvard.edu

ABSTRACT

We present combined single-dish and interferometric CS(2–1) and N₂H⁺(1–0) observations of a compact core in the NW region of the Serpens molecular cloud. The core is starless according to observations from optical to millimeter wavelengths and its lines have turbulent widths and “infall asymmetry”. Line profile modeling indicates supersonic inward motions $v_{\text{in}} \gtrsim 0.34 \text{ km s}^{-1}$ over an extended region $L > 12000 \text{ AU}$. The high infall speed and large extent exceeds the predictions of most thermal ambipolar diffusion models and points to a more dynamical process for core formation. A short (dynamic) timescale, $\sim 10^5 \text{ yr} \simeq L/v_{\text{in}}$, is also suggested by the low N₂H⁺ abundance $\sim 1 \times 10^{-10}$.

Subject headings: ISM: individual(Serpens) — ISM: kinematics and dynamics — stars: formation

1. Introduction

Turbulence is a ubiquitous feature of the interstellar medium although its precise nature is poorly understood and its role in the formation of stars is unclear. Theories of isolated star formation generally assert that gravitational collapse occurs onto a thermally supported core (e.g., Shu, Adams, & Lizano 1987) and motions are quasi-static until very late times (Basu & Mouschovias 1994; Ciolek & Mouschovias 1995; Li 1998). Observations of infall at small scales ($\sim 0.01 \text{ pc}$) in the isolated starless core, L1544, in Taurus are not in contradiction with such theories if it is indeed sufficiently close to forming a star (Williams et al. 1999), although large scale motions ($\gtrsim 0.1 \text{ pc}$) do appear to require an alternative explanation (Tafalla et al. 1998), such as turbulent dissipation (Myers & Lazarian 1998).

¹Current address: National Radio Astronomy Observatory, Campus Building 65, 949 N. Cherry Avenue, Tucson, AZ 85721-0665; jpwilliams@nrao.edu

The Serpens molecular cloud (d=310 pc; de Lara, Chavarria-K, & Lopez-Molina 1991) has more embedded YSOs and is more turbulent than the Taurus cloud. In the northwest region of this cloud lies a cluster of Class 0 sources (Hurt & Barsony 1996) which has been the subject of numerous studies in the millimeter and sub-millimeter regime (Casali, Eiroa, & Duncan 1993; McMullin et al. 1994; White et al. 1995; Hurt, Barsony, & Wootten 1996; Wolf-Chase et al. 1998; Testi & Sargent 1998). Since the dense cores around Class 0 sources often show the spectral signature of inward motion (Mardones et al. 1997), we embarked on a study of the dense gas dynamics in this young cluster forming region in order to compare with more isolated star forming sites such as in Taurus. In this *Letter*, we present observations of a previously unrecognized core adjacent to the Class 0 source S68N that appears to be starless, contracting, and is highly turbulent. We compare its properties with its neighbor, S68N, deduce a chemical timescale for its formation that suggests that it is very young, and determine an average infall speed by spectral line modeling. This core, which we designate S68NW, demonstrates that turbulent motions in the ISM cannot be ignored in the formation of individual stars in clusters.

2. Observations

A well tested method of diagnosing inward motions onto a star forming region is to search for self-absorbed lines where emission at low velocities is brighter than at high velocities (Leung & Brown 1977; Walker et al. 1986; Zhou et al. 1993). We observed CS(2–1) and N₂H⁺(1–0) toward the cluster of Class 0 sources since both lines are reasonably bright hence quick to map, both are strongly excited by gas of density $n_{\text{H}_2} \sim 10^5 \text{ cm}^{-3}$, and generally CS is optically thick and N₂H⁺ is optically thin at the resolution of these observations.

Singledish maps were made at the Five College Radio Astronomy Observatory² (FCRAO) 14 m telescope in December 1996 using the QUARRY 15 beam array receiver and the FAAS backend consisting of 15 autocorrelation spectrometers with 1024 channels set to an effective resolution of 24 kHz (0.06 km/s). The observations were taken in frequency switching mode and, after folding, 3rd order baselines were subtracted. The pointing and focus were checked every 3 hours on nearby SiO maser sources. The FWHM of the telescope beam is 50'', and a map covering 6' × 8' was made at Nyquist (25'') spacing.

Observations were subsequently made with the 10 antenna Berkeley-Illinois-Maryland

²FCRAO is supported in part by the National Science Foundation under grant AST9420159 and is operated with permission of the Metropolitan District Commission, Commonwealth of Massachusetts

array³ (BIMA) for two 8 hour tracks in each line during April 1997 (CS) and October/November 1997 (N_2H^+). A two field mosaic was made with phase center $\alpha(2000) = 18^{\text{h}}29^{\text{m}}47\overset{\text{s}}{.}5$, $\delta(2000) = 01^{\circ}15'51\overset{\text{s}}{.}4$ and a second slightly overlapping pointing at $\Delta\alpha = 33\overset{\text{s}}{.}0$, $\Delta\delta = -91\overset{\text{s}}{.}0$. Amplitude and phase were calibrated using 4 minute observations of 1751+096 (4.4 Jy) interleaved with each 22 minute integration on source. The correlator was configured with two sets of 256 channels at a bandwidth of 12.5 MHz (0.15 km s⁻¹ per channel) in each sideband and a total continuum bandwidth of 800 MHz. The flexible correlator setup allowed us to observe $\text{CH}_3\text{OH}(2_1 - 1_1)$ in addition to CS(2–1), and C³⁴S(2–1) along with $\text{N}_2\text{H}^+(1-0)$: the methanol line was found to map the outflow associated with S68N (Wolf-Chase et al. 1998) but the C³⁴S line was detected only marginally.

The data were calibrated and maps produced using standard procedures in the MIRIAD package. Since the emission is extended, analysis of the spectra must correct for the spatial filtering properties of the interferometer. To allow for this, we combined the FCRAO and BIMA data using the task IMMERGE. Maps were compared within the region of visibility overlap (6 m to 14 m) and small pointing corrections made to the FCRAO data (< 6'', about a tenth of the beam) which was then scaled using a gain of 43.7 Jy K⁻¹.⁴ The resolution of the resulting maps was $10\overset{\text{s}}{.}0 \times 7\overset{\text{s}}{.}8$ at p.a. -72° for CS which was observed twice in the compact C configuration and $8\overset{\text{s}}{.}5 \times 4\overset{\text{s}}{.}6$ at p.a. $+2^{\circ}$ for N_2H^+ which was observed once in C configuration and once in the wider B configuration.

3. Analysis

3.1. S68N and S68NW

Analysis of the large scale maps is deferred to a later paper. Here, we restrict attention to a remarkable region, $\sim 1\overset{\text{s}}{.}5 \times 2'$, around the S68N protostar. This source was discovered from earlier 3-element BIMA CS observations by McMullin et al. (1994) but we re-observed it with the 10-element array to obtain greater sensitivity and resolution. It was originally undetected in the 3 mm continuum but is readily apparent in the new data at an integrated flux level of 12.3 mJy, in agreement with OVRO observations by Testi & Sargent (1998). S68N has also been detected at shorter wavelengths and its spectrum was fit by a modified

³Operated by the University of California at Berkeley, the University of Illinois, and the University of Maryland, with support from the National Science Foundation

⁴Information regarding aperture efficiency measurements on the FCRAO 14 m telescope can be found on the World Wide Web at <http://donald.phast.umass.edu/~fcrao/library/techmemos/gain96.html>

blackbody with dust temperature 20 K and luminosity $5 L_{\odot}$ by Wolf-Chase et al. (1998).

Maps of the integrated intensity of CS(2–1) and N₂H⁺(1–0) around S68N are displayed in Fig. 1. The position of the 3 mm continuum peak, indicated by the star, lies at the center of the N₂H⁺ emission but is offset by 7" from the CS core. However, there is both high velocity emission from the outflow and self-absorption present in the CS spectra which may skew the map of integrated intensity relative to the distribution of dense gas around the star.

Equally striking in the CS map, however, is the presence of a compact core, hereafter S68NW, that lies $\sim 50''$ west of S68N. It is also present in the map of N₂H⁺ integrated intensity but is not nearly so prominent. It was not detected in the continuum to a 3σ sensitivity of 3.3 mJy beam⁻¹, nor is it apparent in the slightly higher sensitivity OVRO Testi & Sargent observations. It is also undetectable in maps at 1 mm (Casali et al. 1993; Tafalla & Mardones, private communication), at 12, 25, 60, and 100 μ m in the Hurt & Barsony IRAS HIRES maps, in the near-infrared (2 μ m; Eiroa & Casali 1992) or in the Digital Sky Survey. These observations constrain the luminosity of any embedded object in S68NW to be less than $0.5 L_{\odot}$.

3.2. Abundance differences

Fig. 1 suggests a difference in the chemistry between the star forming S68N and starless S68NW core. We have estimated the abundance of N₂H⁺ in the two cores by comparing the mass of N₂H⁺ derived from the integrated emission with the virial mass derived from the size and linewidth. Given the compact appearance of the cores, the assumption of virialization is unlikely to be greatly in error. We define the boundaries of each core as the FWHM contour of the N₂H⁺ maps and calculate sizes, linewidths, and integrated emission within these limits. Core properties are listed in Table 1.

The inferred virial N₂H⁺ abundance is much lower in S68NW than S68N. This is due to a combination of a smaller size, greater linewidth, and lower integrated intensity in S68NW, but the relatively low emission is the dominant factor. In the following section, infall model fits do not find such an extreme abundance difference between the two but nevertheless confirms that the N₂H⁺ abundance in S68NW is unusually low, $\sim 1 \times 10^{-10}$, compared to $\sim 4 \times 10^{-10}$ in other dense cores (Womack, Ziurys, & Wyckoff 1992; Ungerechts et al. 1997). A potential explanation that suits the starless nature of S68NW is chemical evolution: Bergin et al. (1997) show that whereas CS forms very quickly in a dense core, it takes $\gtrsim 10^5$ yr to form substantial amounts of N₂H⁺. Observations of other time-sensitive molecular species such as HC₃N offer a test of this hypothesis.

3.3. Spectral line modeling

The majority of the CS spectra in this region are double-peaked and the magnitude of the dips between the peaks tends to increase closer to the core centers. Average spectra within the FWHM contour of N_2H^+ emission for each core are displayed in Fig. 2. Unlike the case of L1544 (Williams et al. 1999), the N_2H^+ spectra are not self-absorbed and we use these data to determine the velocity and linewidth of the cores. For each core, the central dip in the CS spectrum lines up with the N_2H^+ velocity indicating that the CS emission is self-absorbed. The S68N spectrum shows prominent outflow wings but it is quite symmetric in marked contrast to S68NW for which the lower velocity (blue) peak is much brighter than the higher velocity (red) peak. For a radially decreasing excitation gradient, such as would exist for a centrally condensed core at constant kinetic temperature, this indicates that the outer self-absorbing gas is red-shifted (i.e., infalling) relative to the inner emitting region.

To estimate the speed of the infalling gas, we have fit the spectra using a simple two layer model consisting of two isothermal layers, the near side (to the observer) at low density and the far side at high density. This model resembles those discussed by Myers et al. (1996) and Williams et al. (1999): emission from the rear layer is absorbed by the lower excitation front layer with the location of the absorption dependent on the relative velocity between the front and rear layers (i.e., the infall speed). Observations are used to constrain the models as much as possible: gaussian fits to the isolated N_2H^+ hyperfine component are used to set the systemic velocity and linewidth of the core, the line-of-sight widths of each layer are set equal to the measured radius of the cores, and the N_2H^+ abundances are constrained to vary only within a factor of two of the virial estimates derived in the previous section. The free parameters are the densities of each layer, their common kinetic temperature, the molecular abundances, and the infall speed of the front layer onto the rear layer. In addition, a low optical depth component between the two layers was added to the S68N model to allow for the outflow, and a gaussian component $\sim 2 \text{ km s}^{-1}$ from line center was used in the S68NW model to fit excess emission at low velocities.

The model spectra are shown in relation to the observations in Fig. 2 and model parameters listed in Table 2. The rear layer densities are very similar, approximately equal to the critical density of the two transitions, and the foreground layer densities are comparable to each other and similar to the density of ^{13}CO emitting gas. The kinetic temperatures are the same for both cores and equal to the dust temperature of S68N as determined from the spectral energy distribution by Wolf-Chase et al. (1998). The CS abundances are also the same and consistent with observations of Orion by Ungerechts et al. (1997) but the fits require a smaller difference in N_2H^+ abundance than the virial estimates derived in the previous section (note, however, that the N_2H^+ abundance of S68NW is still very low). The

parameter that is most different between the two cores is the infall speed. The low infall speed in S68N is implied by the near symmetry of the line profile and is little affected by the addition of the outflow component which is also quite symmetrical. The inferred infall speed for S68NW, however, is high because of the large blue-red asymmetry but its precise value is very sensitive to the strength of an additional gaussian component added at low velocities. This extra component appears to be physically unrelated to S68NW; it lacks a red counterpart and peaks in emission $\sim 2 \text{ km s}^{-1}$ from the N_2H^+ line. Channel maps suggest that it is a second CS core, slightly offset along the line of sight. Its contribution to the integrated CS intensity within one linewidth of the central velocity of N_2H^+ is less than 20% at its peak and is generally much less in other spectra. The addition of this extra component reduces the blue-red ratio required in the infall model resulting in a smaller infall speed: in the absence of this component, the inferred infall speed is $\gtrsim 0.5 \text{ km s}^{-1}$. Therefore, we believe that the value listed in Table 2, 0.34 km s^{-1} , is a *lower limit* which implies that the S68NW core is contracting supersonically ($v_{\text{in}}/\sigma_{\text{thermal}}(\text{H}_2) > 1$) although not necessarily super-Alfvénically ($v_{\text{in}}/\sigma_{\text{non-thermal}} \gtrsim 0.5$). The implied mass infall rate of the front layer onto the rear layer is $1 \times 10^{-7} M_{\odot} \text{ yr}^{-1}$.

4. Discussion

The data presented here indicate that S68NW is a turbulent core in the process of contraction and increasing its mass substantially. Furthermore its proximity to the S68N core and embedded protostar suggests that S68NW may soon form a low-mass star, as the next part of the sequence of low-mass star formation events which have occurred in the Serpens complex over the last Myr. If so, the formation of stars and cores in Serpens may substantially overlap in time, in contrast to the idea that star formation in clusters is coeval, such as in response to a single triggering event (e.g. Zinnecker, McCaughrean & Wilking 1993). Instead these observations imply that the cloud is forming a core while its already formed cores are still forming stars. If so, core formation and star formation may have relatively similar timescales, each shorter than the overall cluster formation timescale.

The instantaneous collapse timescale, $t_{\text{coll}} = 6200 \text{ AU}/0.34 \text{ km s}^{-1} \simeq 10^5 \text{ yr}$ is approximately equal to the free-fall time for gas of density $n(\text{H}_2) \sim 10^5 \text{ cm}^{-3}$. Such dynamic motions are achieved in models of ambipolar diffusion only at very late times, $\sim 10^7 \text{ yr}$ (Basu & Mouschovias 1994; Ciolek & Mouschovias 1995; Li 1998), which appears to be inconsistent with the low N_2H^+ abundance. In addition, the supersonic infall speed requires either low ionization levels, $x_e < 10^{-8}$ at $n(\text{H}_2) = 3 \times 10^4 \text{ cm}^{-3}$ (Basu & Mouschovias 1995a), significantly less than measured in cores in Taurus (Williams et al. 1998) and Orion

(Bergin et al. 1999), or a weak magnetic field, $B \lesssim 10 \mu\text{G}$ at $n(\text{H}_2) = 5 \times 10^3 \text{ cm}^{-3}$ (Basu & Mouschovias 1995b) which would imply a smaller Alfvén speed, $\sim 0.2 \text{ km s}^{-1}$, than the observed linewidth. Such a weak field at these relatively high densities may also conflict with HI Zeeman measurements of similar size fields at much lower gas densities in Ophiuchus (Goodman & Heiles 1994). Finally, ambipolar diffusion models do not predict the large size scales over which infall occurs: asymmetric, self-absorbed CS line profiles extend well beyond the FWHM N_2H^+ contour, indicating detectable inward motions over $\gtrsim 0.1 \text{ pc}$. Similarly large infall zones have also been observed in the isolated core L1544 (Tafalla et al. 1998) and in the cluster forming regions, L1251B and NGC1333-IRAS4 (Mardones 1998).

A possible explanation is that the collapse front propagates outward at the non-thermal, rather than the thermal, sound speed (e.g. Myers & Fuller 1993) in which case the ratio of infall speed to effective sound speed remains comfortably within the bounds of ambipolar diffusion models. However, this requires that the non-thermal motions be maintained in the core over the ambipolar diffusion timescale, $t_{\text{AD}} \simeq 10^6 \text{ yr}$, but Nakano (1998) shows that the timescale for turbulent dissipation is approximately the same as the free fall time and much less than t_{AD} in the absence of any internal driving sources. Indeed, it may be the decay of the non-thermal motions, with a corresponding loss of pressure support, that drives the fast inward motions in S68NW (Myers & Lazarian 1998) over the large observed size scales. Although we do not observe a decrease in the N_2H^+ velocity dispersion toward S68NW, this does not preclude the existence of a small less turbulent central core. Observing such an object remains a challenge for the future. Note that in this scenario, the timescale of the next stage of star formation would be that of ambipolar diffusion if the core were magnetically subcritical, or would be dynamical if the core were magnetically supercritical. It will be useful to determine the incidence of cores like S68NW in other star-forming regions, and to study such cores in lines sensitive to a wide range of gas density.

This research was partially supported by NASA Origins of Solar Systems Program, grant NAGW-3401. JPW thanks the Radio Astronomy Laboratory at the University of California at Berkeley for support during the writing of the manuscript and Chris McKee and Frank Shu for informative discussions. Conversations with Shantanu Basu, Glenn Ciolek, and Zhi-Yun Li are also gratefully acknowledged.

REFERENCES

- Basu, S., & Mouschovias, T.C. 1994, ApJ, 432, 720
- Basu, S., & Mouschovias, T.C. 1995a, ApJ, 452, 386
- Basu, S., & Mouschovias, T.C. 1995b, ApJ, 453, 271

Bergin, E.A., Goldsmith, P.F., Snell, R.L., & Langer, W.D. 1997, *ApJ*, 482, 285
Bergin, E.A., Plume, R., Williams, J.P., & Myers, P.C. 1999, *ApJ*, 512, 724
Casali, M.M., Eiroa, C., & Duncan, W.D. 1993, *A&A*, 275, 195
Ciolek, G.E., & Mouschovias, T.C. 1995, *ApJ*, 454, 194
de Lara, E., Chavarria-K, C., & Lopez-Molina, G. 1991, *A&A*, 243, 139
Eiroa, C., & Casali, M.M. 1992, *A&A*, 262, 468
Goodman, A.A., & Heiles, C. 1994, *ApJ*, 424, 208
Hurt, R.L., & Barsony, M. 1996, *ApJ*, 460, L45
Hurt, R.L., Barsony, M., & Wootten, A. 1996, *ApJ*, 456, 686
Leung, C.M., & Brown, R.B. 1977, *ApJ*, 214, L73
Li, Z.-Y. 1998, *ApJ*, 493, 230
Mardones, D. 1998, Ph.D. Thesis, Harvard University
Mardones, D., Myers, P.C., Tafalla, M., Wilner, D.J., Bachiller, R., & Garay, G. 1997, *ApJ*, 489, 719
McMullin, J.P., Mundy, L.G., Wilking, B.A., Hezel, T., & Blake, G. 1994, *ApJ*, 424, 222
Myers, P.C., & Fuller, G.A. 1993, *ApJ*, 402, 635
Myers, P.C., Mardones, D., Tafalla, M., Williams, J.P., Wilner, D.J. 1996, *ApJ*, 465, L133
Myers, P.C., & Lazarian, A. 1998, *ApJ*, 507, L157
Nakano, T. 1998, *ApJ*, 494, 587
Shu, F.H., Adams, F.C., & Lizano, S. 1987, *A.R.A&A.*, 25, 23
Tafalla, M., Mardones, D., Myers, P.C., Caselli, P., Bachiller, R., & Benson, P.J. 1998, *ApJ*, 504, 900
Testi, L., & Sargent, A.I. 1998, *ApJ*, 508, L91
Ungerechts, H., Bergin, E. A., Goldsmith, P. F., Irvine, W. M., Schloerb, F. P., & Snell, R. L. 1997, *ApJ*, 482, 245
Walker, C.K., Lada, C.J., Young, E.T., Maloney, P.R., & Wilking, B.A. 1986, *ApJ*, 309, L47
White, G.J., Casali, M.M., & Eiroa, C. 1995, *A&A*, 298, 594
Williams, J.P., Bergin, E.A., Caselli, P., Myers, P.C., & Plume, R. 1998, *ApJ*, 503, 689
Williams, J.P., Myers, P.C., Wilner, D.J., & Di Francesco, J. 1999, *ApJ*, 513, L61
Wolf-Chase, G.A., Barsony, M., Wootten, H.A., Ward-Thompson, D., Lowrance, P.J., Kastner, J.H., & McMullin, J.P. 1998, 501, L193
Womack, M., Ziurys, L.M., & Wyckoff, S. 1992, *ApJ*, 387, 417
Zhou S., Evans, N.J., Kömpe, C., & Walmsley, C.M. 1993, *ApJ*, 404, 232
Zinnecker, H., McCaughrean, M.J., & Wilking, B.A. 1993, in *Protostars and Planets III*, eds. E. Levy, J.I. Lunine, & M.S. Matthews (Tucson: U. of Arizona Press), 429

TABLE 1
 $\text{N}_2\text{H}^+(1-0)$ Core Comparison

	S68N	S68NW
FWHM Radius (AU)	8100	6200
FWHM Linewidth (km s ⁻¹)	0.95	1.50
Virial Mass ^a (M_\odot)	4.5	8.4
Integrated Intensity (K km s ⁻¹)	15.1	5.8
Abundance ^b ($\times 10^{-10}$)	5.6	0.66

^a for an inverse square density profile

^b relative to H₂, $T_{\text{ex}} = 15$ K

TABLE 2
 Infall model parameters

	S68N	S68NW
Rear layer density (cm ⁻³)	2.1×10^5	2.2×10^5
Front layer density (cm ⁻³)	1.0×10^3	2.1×10^3
Kinetic temperature (K)	20.0	20.0
CS abundance ^a ($\times 10^{-9}$)	8.0	8.0
N_2H^+ abundance ^a ($\times 10^{-10}$)	2.8	1.1
Infall speed (km s ⁻¹)	0.01	0.34

^a relative to H₂

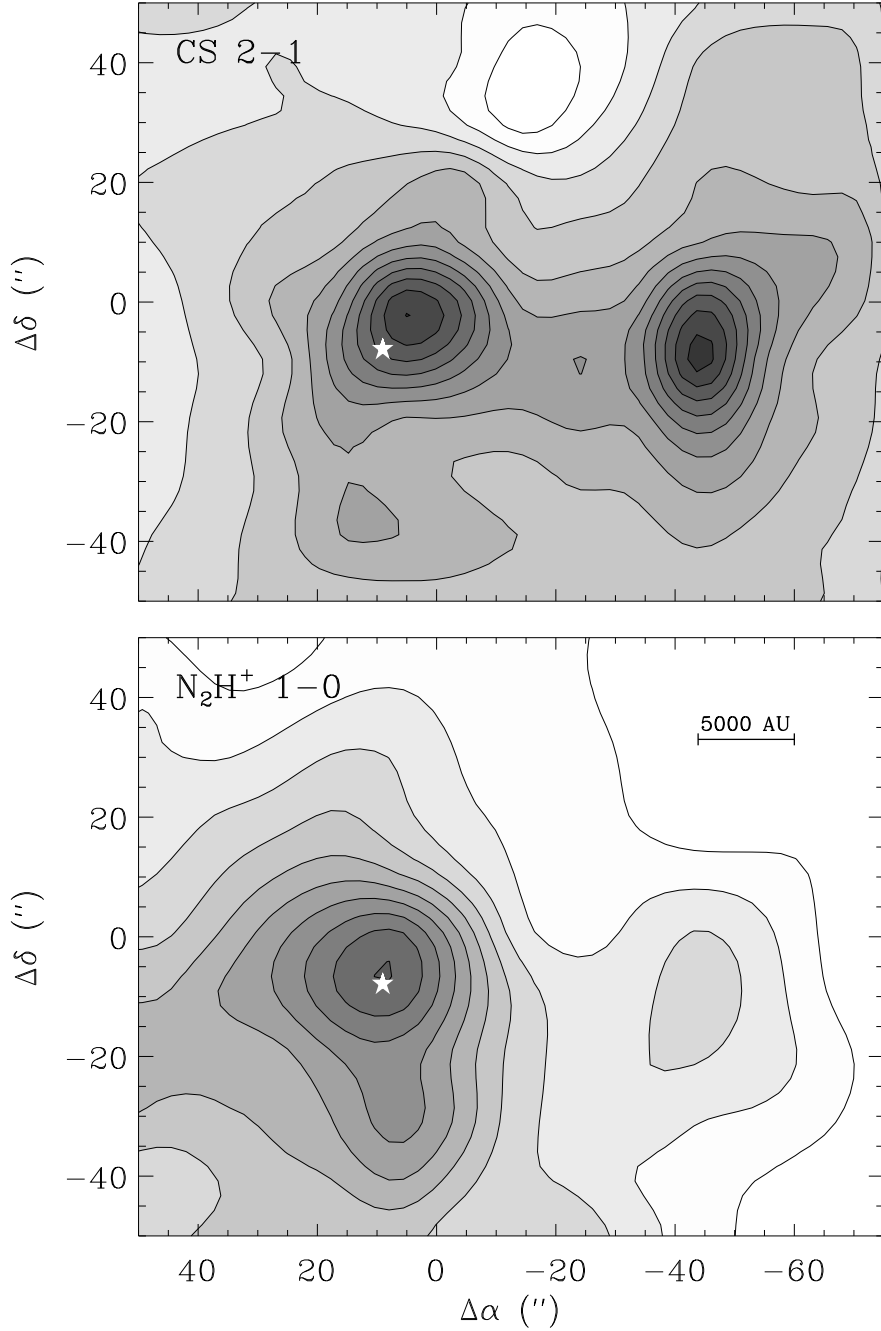


Fig. 1.— Combined FCRAO/BIMA maps of CS(2–1) and N₂H⁺(1–0) of the S68N and S68NW cores. The position of the 3 mm continuum source (S68N) is marked. Offsets are relative to $\alpha(2000) = 18^{\text{h}}29^{\text{m}}47\overset{\text{s}}{.}5$, $\delta(2000) = 01^{\circ}15'51\overset{\text{s}}{.}4$. Both maps have been smoothed to a resolution of 10''. Contour starting level and increments are 2.0 and 0.5 K km s^{−1} for the CS and N₂H⁺ map respectively.

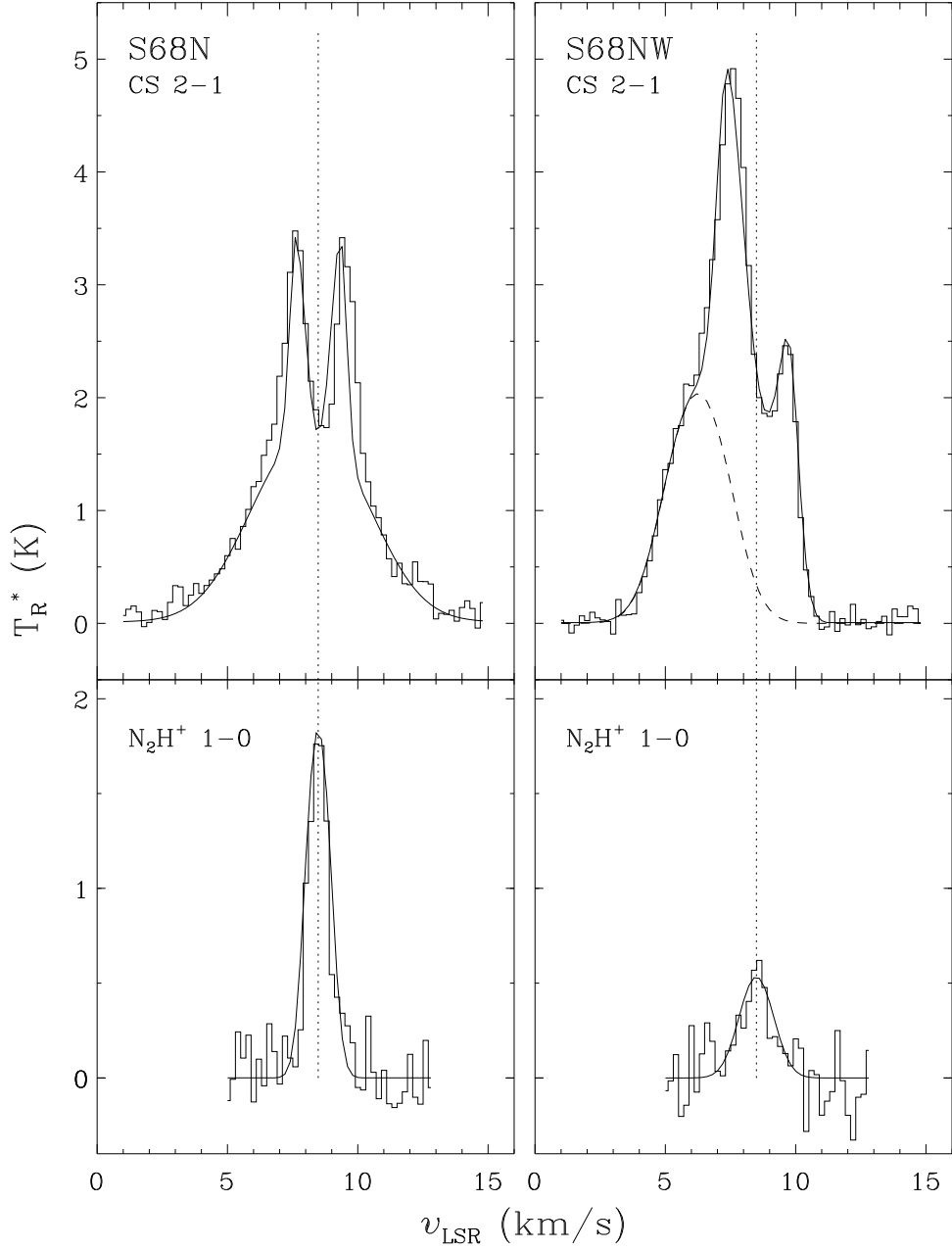


Fig. 2.— Spectra of the S68N and S68NW cores, averaged over over the N_2H^+ integrated intensity FWHM contour. The central velocity of N_2H^+ was measured from a gaussian fit to the isolated hyperfine component ($F_1F = 01 - 12$) and is indicated by the dotted line. Model fits, consisting of two layers in relative motion, are shown by the continuous line. An outflow component has been added to the S68N model to account for the high velocity wing emission, and an unrelated gaussian component (dashed line) to the S68NW model to account for additional emission at low velocities.